

Performance of ESPRESSO's high resolution 4x2 binning for characterizing intervening absorbers towards faint quasars

Trystyn A. M. Berg^{1,2,*}, Guido Cupani³, Pedro Figueira^{1,4}, and Andrea Mehner¹

¹ European Southern Observatory, Alonso de Cordova, 3107, Casilla, 19001, Santiago, Chile

² Departamento de Astronomía, Universidad de Chile, Casilla, 36-D, Santiago, Chile

³ INAF-Osservatorio Astronomico di Trieste, Via Tiepolo 11, I-34143, Trieste, Italy

⁴ Instituto de Astrofísica e Ciências do Espaço, Universidade do Porto, CAUP, Rua das Estrelas, 4150-762, Porto, Portugal

May 11, 2022

ABSTRACT

As of October 2021 (Period 108), the European Southern Observatory (ESO) offers a new mode of the ESPRESSO spectrograph designed to use the High Resolution grating with 4×2 binning (spatial by spectral; HR42 mode) with the specific objective of observing faint targets with a single Unit Telescope at Paranal. We validated the new HR42 mode using four hours of on-target observations of the quasar J0003-2603, known to host an intervening metal-poor absorber along the line of sight. The capabilities of the ESPRESSO HR42 mode (resolving power $R \approx 137\,000$) were evaluated by comparing to a UVES spectrum of the same target with a similar integration time but lower resolving power ($R \approx 48\,000$). For both data sets we tested the ability to decompose the velocity profile of the intervening absorber using Voigt profile fitting and extracted the total column densities of C IV, N I, Si II, Al II, Fe II, and Ni II. With $\approx 3\times$ the resolving power and $\approx 2\times$ lower S/N for a nearly equivalent exposure time, the ESPRESSO data is able to just as accurately characterize the individual components of the absorption lines as the comparison UVES data, but has the added bonus of identifying narrower components not detected by UVES. For UVES to provide similar spectral resolution ($R > 100\,000$; $0.3''$ slit) and the broad wavelength coverage of ESPRESSO, the Exposure Time Calculator (ETC) supplied by ESO estimates 8 hrs of exposure time spread over two settings; requiring double the time investment than that of ESPRESSO's HR42 mode whilst not properly sampling the UVES spectral resolution element. Thus ESPRESSO's HR42 mode offers nearly triple the resolving power of UVES ($0.8''$ slit to match typical ambient conditions at Paranal) and provides more accurate characterization of quasar absorption features for an equivalent exposure time.

Key words. Instrumentation: spectrographs, Quasars: absorption lines, Galaxies: abundances

1. Introduction

Gaseous systems seen in absorption along quasar sightlines are excellent probes of astrophysics throughout cosmic time, from measuring the physical and chemical evolution of gaseous reservoirs of galaxies (Berg et al. 2015; Neeleman et al. 2015; Noterdaeme et al. 2021) to imposing constraints on dark matter properties (Iršič et al. 2017) and fundamental constant evolution in our Universe (e.g., Murphy & Cooksey 2017; Schmidt et al. 2021). Accurately quantifying these probes requires a detailed kinematic decomposition of all absorption lines along a quasar sightline. For distinct QSO absorption line systems (QALs), the metal absorption profiles are often quite complex, consisting of several sub-components (with a typical width between $\approx 5 - 100 \text{ km s}^{-1}$) spread out over a few hundred km s^{-1} . In addition, the neutral hydrogen absorption of individual absorbers are sometimes significantly blended within the Ly α forest absorption from the intervening intergalactic medium. While low resolution spectra (with resolving power $R < 1000$) can easily identify the strongest Ly α QALs such as damped Lyman α systems (DLAs; H I column densities of $\geq 2 \times 10^{20} \text{ atom cm}^{-2}$; Wolfe et al. 2005), spectrographs like UVES (Dekker et al. 2000) are frequently used to identify the weaker H I absorbers, which are required to probe the intergalactic and circumgalactic media. Typical studies of faint quasars with UVES use a $1''$ slit

($R \approx 48\,000$) to maximize R while minimizing light loss based on the median seeing of Paranal ($\approx 0.8''$).

Although UVES has proved to be an effective instrument for the study of QALs over the past 20 years, the QAL community are now exploring higher spectral resolving power ($R \gtrsim 100\,000$; i.e., the smallest cloud widths of $\gtrsim 3 \text{ km s}^{-1}$) to pinpoint the detailed structure of the absorption line profiles, and search for rarely detected species, such as: (i) deuterium and lithium for constraining Big Bang nucleosynthesis (Cooke et al. 2018), (ii) molecular hydrogen to constrain the gas and dust properties of high redshift galactic gas reservoir (Tchernyshyov et al. 2015; De Cia 2018; Krogager et al. 2018), and (iii) exotic nucleosynthetic species to place constraints on chemical evolution processes (Ellison et al. 2002; Berg et al. 2013). To do these experiments with UVES would require the smallest slit widths ($0.3''$; thus $R \approx 100\,000$), leading to large amounts of light loss at the slit interface unless observations are completed in the most pristine atmospheric seeing conditions. In essence, it is not efficient for UVES to continue to explore the emerging questions of the QAL community.

The ESPRESSO spectrograph (Pepe et al. 2010, 2021) provides an excellent alternative to UVES for observing QALs at high spectral resolution. In its medium-resolution mode, the 4 Unit Telescope (UT) MULTIMR42 mode ($R = 75\,000$ with 4×2 binning), ESPRESSO has already proven to be effective at using QALs to constrain our understanding of the Universe (Cooke

* tberg@eso.org

et al. 2020; Welsh et al. 2020). However, these observations require all 4 UTs simultaneously, and the collection of light from MULTIMR42 mode means a reduction of R from $\approx 137\,000$ to $75\,000$; a resolution UVES can obtain without excessive slit losses in average Paranal atmospheric conditions. As of Period P108, ESPRESSO supports a single UT mode with 4×2 binning (HR42 mode). This mode is designed to reduce read-out noise while maintaining a high spectral resolving power ($R \approx 137\,000$) and is ideal for observing faint targets such as QSOs.

In this paper, we present the results from a pilot program to test the ability of ESPRESSO’s HR42 mode to analyze the chemical contents of a DLA seen along a quasar sightline, and compare the performance of ESPRESSO HR42 mode to the typical observing set-up used for UVES.

2. Target selection, observations and data reduction

The target, QSO J0003–2603 (right ascension 00 hr 03’ 22.953”, declination $-26^\circ 03' 18.307''$, and redshift $z_{\text{em}} = 4.01$), was chosen as it is: (i) sufficiently bright for the ESPRESSO autoguiding system (AB magnitude $R = 18.5$ mag), (ii) known to host an intervening metal-poor ($[M/H] \approx -2$) DLA absorber along the line of sight (redshift $z_{\text{abs}} = 3.39$, and (iii) has archival UVES observations allowing a direct comparison between instruments (Molaro et al. 2000; Levshakov et al. 2000).

The ESPRESSO observations were carried out on October 2nd 2021 on UT2 at Paranal (Program ID 60.A-9801(W)). Four sequential 60-minute on-target exposures were taken. The observations were made in average seeing conditions ($\approx 0.77''$; image quality at 5000 Å of $\approx 0.85''$) across the four hours of observations at an average airmass of 1.05. The data were reduced with the default settings of the ESPRESSO ESO-reflex pipeline (version 2.3.3; Pepe et al. 2021; Freudling et al. 2013) and post-processed with the ESPRESSO data analysis software (hereafter DAS; version 1.3.3; Cupani et al. 2019; Pepe et al. 2021). While we use the sky-subtracted data in this paper to avoid skyline contribution, we point out that the S/N is marginally better in the spectrum without sky subtraction. The S/N (in units of pixel^{-1} ; $\approx 1\text{ km s}^{-1}$ per pixel) is ≈ 20 within the Ly α forest, and ≈ 30 beyond the Ly α emission line of the quasar.

The quoted resolving power of the HR42 mode, based on the ThAr arc calibrations taken by ESO, is $R \approx 131\,000$. To compare what was achieved by our data, we quantified R using the telluric lines from two different methods. We first assumed that the measured full width half maximum (FWHM) of a weak, unresolved telluric line is equal to the FWHM of the resolution element (FWHM_{res}); the measured FWHM_{res} of the telluric line at $\approx 7685\text{ Å}$ within the median-combined spectrum is $2.269 \pm 0.292\text{ km s}^{-1}$ (corresponding to $R \approx 132\,100$). However, this method assumes that telluric lines are unresolved by ESPRESSO, which is not necessarily true given the high spectral resolution of the HR42 mode. To confirm the specific telluric line was unresolved and to obtain a second, independent measurement of the resolving power, we fitted the telluric lines using MOLECFIT (Smette et al. 2015), which provides both an estimate of FWHM_{res} as well as the intrinsic FWHM of the telluric line based on a model atmosphere at the time of observations. Taking the mean value from each individual exposure, the MOLECFIT-estimated intrinsic FWHM of the telluric line at $\approx 7685\text{ Å}$ is $1.480 \pm 0.050\text{ km s}^{-1}$ and $\text{FWHM}_{\text{res}} = 2.193 \pm 0.050\text{ km s}^{-1}$ ($R \approx 136\,700$). It is clear from the results of MOLECFIT that the telluric line at $\approx 7685\text{ Å}$ is marginally unresolved within our dataset. However we caution that depending on the airmass and

atmospheric conditions at time of observations, the telluric lines may be resolvable by ESPRESSO’s HR mode and will not provide an accurate estimate of the resolving power of the instrument. We adopt $R \approx 136\,700$ from MOLECFIT as the best estimate of the resolving power of the HR42 mode.

The comparison archival UVES data used 4.5 hours of on-target exposures, and was combined and continuum normalized by the UVES Spectral Quasar Absorption Database team (SQUAD; Murphy et al. 2019). Observations were executed during the commissioning of UVES (Program ID 60.A-9022(A); slit width $0.9''$ with the DIC2 437+860 instrument setup), and were observed at similar airmass and at various seeing measurements (from $0.34''$ to $2.4''$; mean of $1.0''$ at 5000 Å) across two nights. Using unresolved telluric lines within the data, the obtained FWHM of the spectral resolution element is $\text{FWHM}_{\text{res}} = 5.981 \pm 0.126\text{ km s}^{-1}$ ($R \approx 50\,100$; archival R measurements from ThAr arc lines obtained $R \approx 47\,900$). The UVES pixel size is $\approx 2.5\text{ km s}^{-1}$. The S/N per pixel is $\approx 2\times$ (alternatively, $\approx 1.33\times$ per Å) larger within the UVES spectrum relative to that of ESPRESSO (Figure 1). Once accounting for the difference in pixel size between the two instruments, the S/N of UVES becomes significantly better than ESPRESSO at $\lesssim 5000\text{ Å}$.

3. Results

3.1. Comparison with the ESO Exposure Time Calculator

Figure 1 shows the observed S/N (red line) across the entire spectrum compared to what was estimated using version P109 of the ESPRESSO exposure time calculator (ETC; black points). The ETC S/N estimates have been computed assuming a $0.84''$ image quality, the average airmass through the observations (1.05), and fractional lunar illumination $\text{FLI}=0.0$ as the moon was not visible during observations. The S/N estimated by the ETC is consistently $\approx 1.3\times$ higher across the entire wavelength range. However, we point out that the ETC solely includes emission from the QSO continuum and not absorption lines observed towards QSO J0003–2603 (particularly those of the Ly α forest; $< 6202\text{ Å}$), thus overestimating the estimated S/N. This is particularly demonstrated by the presence of the strong Ly α absorption from the DLA at $z_{\text{abs}} = 3.39$ ($\approx 5300\text{ Å}$ in red line of Figure 1). Using only pixels of the observed ESPRESSO spectrum with predominantly quasar continuum flux near the centers of ESPRESSO’s spectral orders, the observed S/N is only $\approx 1.15\times$ smaller than the ETC predicts.

To obtain a near-equivalent spectrum with UVES (i.e., $R \approx 110\,000$) and wavelength coverage from 3800 Å to 7880 Å , one would need to observe with two UVES settings (e.g., DIC1 390+580 and DIC2 437+760) and with slit widths of $0.3''$. The cyan points in Figure 1 show the ETC-predicted S/N for the UVES spectrum using these two settings and $0.3''$ slit width, with an exposure time of four hours *per setting* under the same observing conditions as the ESPRESSO observations. The S/N of the cyan points is $\approx 2\times$ higher per pixel than what is observed with ESPRESSO for two reasons. First, as there is overlap in wavelength between the two UVES settings, there is an increase in the S/N in the wavelength ranges $\approx 3760\text{--}4480\text{ Å}$, $\approx 4770\text{--}4960\text{ Å}$, and $\approx 5700\text{--}6780\text{ Å}$. Secondly, the UVES unbinned pixel sampling of the resolution element of this setup is 1.39 pixels per element in the blue and 1.94 pixels in the red. Not only does this pixel size lead to under-sampling in the spectral direction, but also it results in an increase in S/N per pixel of $1.18\text{--}1.39\times$ compared to ESPRESSO. Thus the expected ratio of the S/N be-

tween UVES and ESPRESSO – after accounting for the doubled exposure time in overlapping regions of the two UVES settings, and the resolution element size – is between 1.18 and 1.97, and explains the majority of the discrepancy between the red curve and cyan points of Figure 1. While ESPRESSO is expected to be as efficient as UVES with a 0.3" slit to obtain a $R > 100\,000$ spectrum, ESPRESSO is able to obtain full wavelength coverage (3800Å to 7880Å) in a single setup whilst Nyquist sampling the spectral resolution element, making the HR42 mode more efficient in terms of observing time required.

3.2. Characterization of the intervening absorber with ESPRESSO

By simultaneously fitting the continuum and a Voigt profile to both the Ly α and Ly β lines, the measured H I column density of the intervening absorber towards QSO J0003–2603 is $\log N(\text{H I}) = 21.35 \pm 0.12$ at $z_{\text{abs}} = 3.3901$. The measured H I column density is consistent with previous measurements (Lu et al. 1996). The Voigt profile fit to the Ly α absorption line is shown in Figure 2.

Additionally, Voigt profile fitting was done for absorption lines of key metal species (C IV, N I, Si II, Al II, Fe II, Ni II). We note that in the analysis of the UVES data done by Molaro et al. (2000), there was sufficient S/N in the Ly α forest ($\geq 10 \text{ pixel}^{-1}$) to detect the O I lines λ 925 Å and 950 Å (≈ 4115 Å in the observed frame). However, the efficiency of ESPRESSO at blue wavelengths is too poor to be able to accurately model the continuum within the Ly α forest, although it is possible to see evidence of saturation of the O I λ 929 Å and 950 Å lines. Unfortunately, the wavelength coverage of ESPRESSO does not include coverage of Cr II and Zn II at the redshift of the DLA.

The fitting was done using the code ALIS¹, which uses a χ^2 minimization to simultaneously fit the continuum and profile components from a list of starting redshifts (z), the turbulent component of the Doppler broadening parameters (b_{turb}), gas temperature (T_{gas}), and column densities (N ; in units atoms cm^{-2}) for each ionic species. A Gaussian FWHM of 2.193 km s^{-1} is used as the ESPRESSO line spread function in the fitting procedure. As the HR42 mode provides sufficient resolution to possibly constrain gas temperature (Narayanan et al. 2006), we attempted including T_{gas} as a free parameter per absorption component in the fitting process. Despite having a range of ions of varying atomic mass, many lines in this system are blended or saturated preventing a realistic constraint on T_{gas} ; including T_{gas} as a free parameter in the model suggests a purely turbulent medium. In order to obtain an accurate measure of the column densities for all components of each ion, we elect to assume $T_{\text{gas}} = 10\,000$ K, a typical temperature of metal-poor DLAs (Cooke et al. 2015) rather than separately fitting a single Doppler parameter to each ions' component. While assuming a single T_{gas} may not provide accurate measurements of b_{turb} for each component, the Voigt profile fitting procedure will be more precise as the fit is constrained by more data (i.e. multiple ions' probing the same b_{turb}) and effects from atomic mass are properly accounted for. As a result, this will reduce the overall errors in both the Doppler parameter and $\log N$. Furthermore, by deriving b_{turb} for each component, the fitting also breaks the degeneracy between the Doppler parameter and column density for saturated lines, enabling a measurement of the column density for Si II and Al II. We note that repeating the fitting procedure with a T_{gas} within the range of DLA values (i.e. between 1000K

– 100 000K) has little effect on the derived column densities, which remain consistent with the assumed $T_{\text{gas}} = 10\,000$ K column densities. By assuming a fixed T_{gas} , the errors derived from fitting b_{turb} encapsulate the errors on the total Doppler parameter. The high ions (i.e., C IV) and low ions (N I, Si II, Al II, Fe II, and Ni II) were fitted separately, and assuming that the z of each component of the low ions' velocity profile are the same across all species. Given the level of blending and saturation for many of these lines which introduces model degeneracies while fitting all lines simultaneously, the velocity profiles were fitted in several iterations to constrain individual components free of these degeneracies. First, the strongest components at $\approx 0 \text{ km s}^{-1}$ were fitted using the unsaturated Fe II λ 1611 Å and the two redmost lines of the N I λ 1134 Å triplet (λ 1134.4 and 1135.0 Å) to fix b_{turb} , z and $N(\text{Fe II})$ for these two components that cannot be easily determined from the saturated lines. The redshifts of the rest of the profile (five components total) were then fixed using the unblended Fe II λ 1608 Å, before running the fit on the remaining lines to determine the remaining parameters. These ALIS models were subsequently cross-checked with the ESPRESSO DAS; the results of the two methods are in agreement within the uncertainties. The best-fit absorption profile parameters are presented in the top of Table 1, while the velocity profiles and their corresponding fits are shown in the two leftmost columns of Figure 3. For reference, the velocity of each component relative to z_{abs} (Δv) is tabulated in Table 1.

Similarly, we applied the same profile fitting method to the low ions in the UVES data (assuming an instrumental resolution element of 5.981 km s^{-1} ; right column of Figure 3; bottom of Table 1), and detected only four components. Components 2, 3 and 4 of the ESPRESSO fit (Table 1) are separated by $\approx 20 \text{ km s}^{-1}$, and all three components have a b_{turb} below the resolving power of the 0.9" UVES set-up (FWHM $\approx 6.4 \text{ km s}^{-1}$). As component 2 is weaker than the other two components, the asymmetry in the line profile can be detected within the UVES data, while components 3 and 4 cannot be distinguished. Thus, as a result of the $\approx 3\times$ larger spectral resolving power of the HR42 mode, more components with small b_{turb} can be detected with ESPRESSO despite the modest S/N.

Given the strength of the Si II λ 1526 line in the ESPRESSO data, we point out that there appears to be an artefact in the UVES data near the Si II λ 1808 Å line. The profile shape appears shifted blueward in velocity space ($\approx -5 \text{ km s}^{-1}$) with reference to the other lines (right column of Figure 3), leading to a poor fit using the fixed redshift and b_{turb} from the Al II and Fe II lines. The resulting $\log N(\text{Si II})$ is severely inconsistent with the ESPRESSO value. Fitting a separate, independent two-component profile to the Si II 1808 line results in a total column density estimate of $\log N(\text{Si II}) = 15.65$, which is inconsistent with the sum of the components 2, 3 and 4 of the equivalent absorption feature in the ESPRESSO data ($\log N(\text{Si II}) = 15.07 \pm 0.16$).

The same fitting method was also applied to the C IV doublet velocity profiles (Figure 4). The complexity of the C IV absorption profile combined with either the modest S/N of the ESPRESSO or the resolution of the UVES data leads to a degenerate parameter space, requiring anywhere between 10 and 16 components to provide a satisfactory fit. Many of the additional components beyond the initial 10 are much weaker, with either the column density being several orders of magnitude smaller than the total value and thus consistent with the noise, or the components are shallow and/or broad in shape and could be accounted for by modifying the continuum fit. In many cases, these additional components contribute minimally to the total column

¹ <https://github.com/rcooke-ast/ALIS>

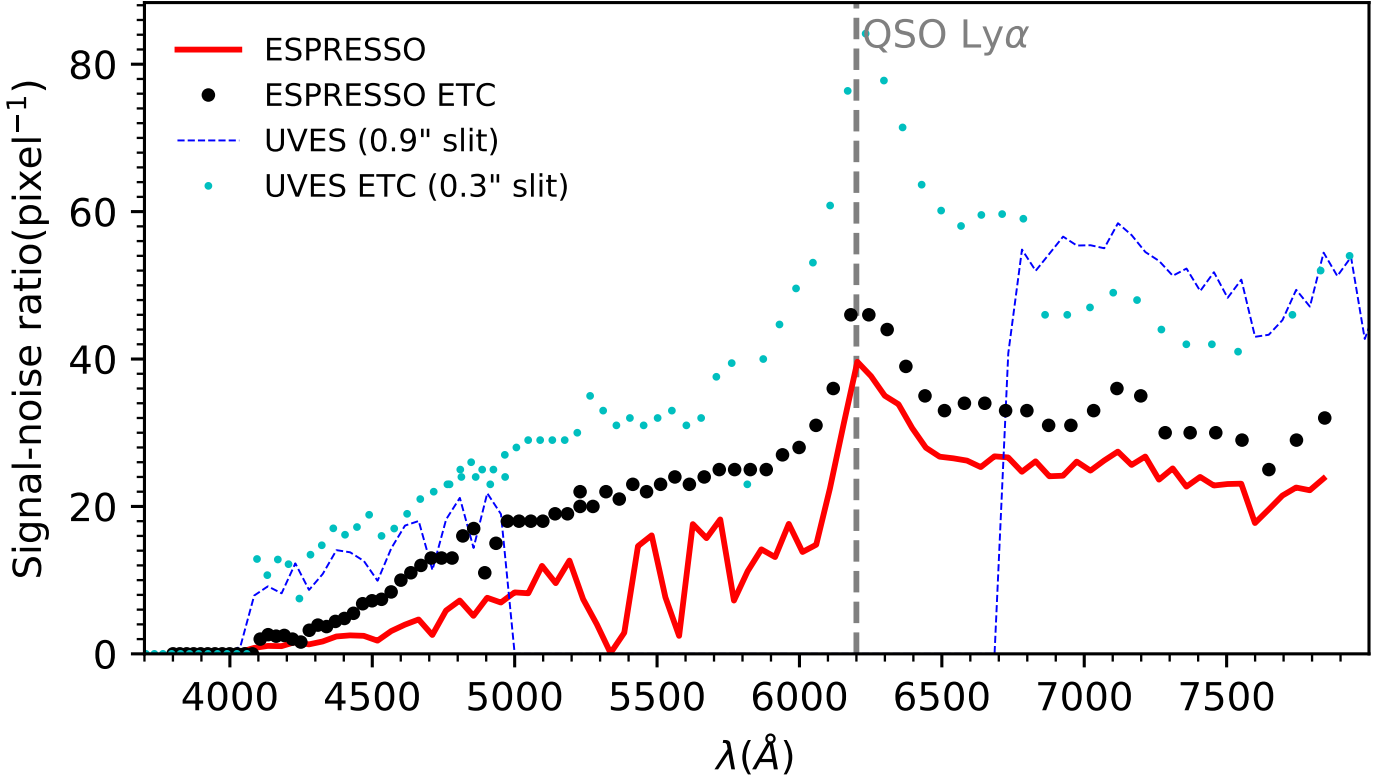


Fig. 1. The S/N (per pixel; $\approx 1 \text{ km s}^{-1}$ per pixel) of the observed ESPRESSO spectrum (solid red line) and ETC-estimated values based on a QSO emission template (black circles). The observed spectrum S/N is estimated as the measured flux divided by the standard deviation from the error spectrum. Note that the red line is smoothed by taking the median S/N within a wavelength bin of the same size as the average space between ETC points. For reference, the vertical grey line denotes the Ly α emission line of the observed QSO. The S/N from the ETC consistently $\lesssim 20$ percent larger than measured in the observations. For reference, the smoothed S/N from the comparison UVES data ($\approx 2.5 \text{ km s}^{-1}$ per pixel) is shown as the blue dotted line. Due to the gaps in the UVES data wavelength coverage, the observed UVES data does not cover the Ly α emission of the QSO. Additionally, the small cyan dots represent the combined ETC estimate for UVES data taken with two UVES settings, with each setting using a $0.3''$ slit (near equivalent R) with the same exposure time *per setting* (i.e., doubled observing time) and observing conditions as the ESPRESSO data.

Table 1. Component Voigt profile fits for low ions

Comp.	z	$\Delta v \text{ (km s}^{-1}\text{)}$	$b_{\text{turb}} \text{ (km s}^{-1}\text{)}$	$\log N(\text{N II})$	$\log N(\text{Si II})$	$\log N(\text{Al II})$	$\log N(\text{Fe II})$	$\log N(\text{Ni II})$
ESPRESSO								
1	3.389512	-42	8.1 ± 0.27	13.25 ± 0.175	...	12.14 ± 0.017	13.38 ± 0.058	12.59 ± 0.271
2	3.389892	-16	4.3 ± 0.09	13.30 ± 0.082	13.71 ± 0.068	12.30 ± 0.017	13.59 ± 0.015	...
3	3.390056	-5	5.1 ± 0.12	14.26 ± 0.021	14.56 ± 0.198	13.17 ± 0.068	14.57 ± 0.026	13.14 ± 0.045
4	3.390188	4	5.1 ± 0.09	14.32 ± 0.019	14.73 ± 0.053	12.86 ± 0.030	14.07 ± 0.015	12.92 ± 0.052
5	3.390481	24	13.7 ± 0.68	...	13.29 ± 0.028	12.06 ± 0.024	12.97 ± 0.062	11.96 ± 0.911
UVES								
1	3.389511	-42	8.4 ± 0.39	12.09 ± 0.054	13.40 ± 0.019	...
2	3.389949	-12	7.0 ± 0.11	...	14.96 ± 0.009	12.79 ± 0.012	13.99 ± 0.008	...
3	3.390130	0	6.5 ± 0.09	...	14.59 ± 0.018	13.29 ± 0.029	14.63 ± 0.018	...
4	3.390505	26	15.4 ± 1.17	11.92 ± 0.035	12.82 ± 0.086	...

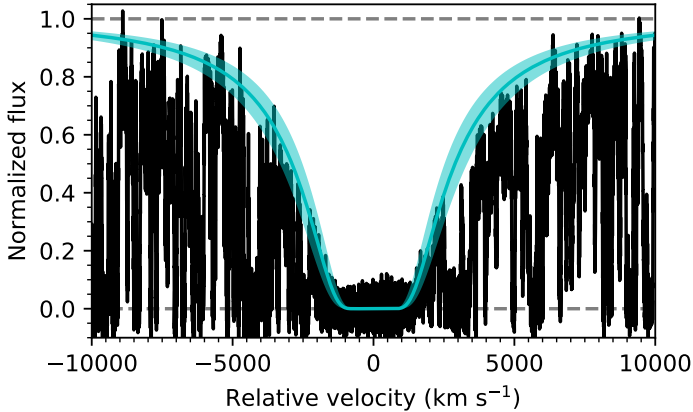
density. For the UVES data, the minimum 10 components were sufficient to reproduce the absorption profile (right column of Figure 4). As with the low ion profile, the ESPRESSO data is able to resolve an additional two components (at $\Delta v = 22$ and 57 km s^{-1} ; left column of Figure 4). The properties of each component for both datasets are tabulated in Table 2. The recovered total column density of C IV from UVES and ESPRESSO are equivalent.

3.3. Comparison of DLA properties between ESPRESSO and UVES

Table 3 provides the total column densities derived from the ESPRESSO and UVES Voigt profile fitting analysis. Errors on the total column densities include continuum fitting errors. Comparing the total column densities derived from ESPRESSO with those from UVES (both from the analysis in this paper and Molaro et al. 2000), all values are consistent. We note that Molaro et al. (2000) only fitted the low ions absorption profile as a sin-

Table 2. Component Voigt profile fits for high ions

Comp.	z	Δv (km s ⁻¹)	b (km s ⁻¹)	$\log N(\text{C iv})$
ESPRESSO				
1	3.388100	-139	11.5 ± 0.17	13.96 ± 0.017
2	3.388645	-101	41.4 ± 1.63	13.76 ± 0.023
3	3.388729	-96	7.5 ± 0.55	13.06 ± 0.039
4	3.389040	-74	12.8 ± 0.78	13.31 ± 0.036
5	3.389703	-29	5.9 ± 0.18	13.22 ± 0.012
6	3.389918	-15	5.4 ± 0.44	13.13 ± 0.067
7	3.390172	3	11.9 ± 1.04	13.91 ± 0.035
8	3.390453	22	8.5 ± 1.42	13.56 ± 0.122
9	3.390717	40	10.3 ± 1.78	13.87 ± 0.082
10	3.390960	57	8.3 ± 1.68	13.55 ± 0.156
11	3.391181	72	9.4 ± 1.09	13.52 ± 0.084
12	3.391497	93	16.2 ± 0.87	13.48 ± 0.031
UVES				
1	3.388094	-139	11.2 ± 0.11	13.95 ± 0.005
2	3.388660	-100	43.3 ± 1.05	13.84 ± 0.015
3	3.388702	-98	4.3 ± 0.42	12.86 ± 0.028
4	3.389022	-76	14.3 ± 0.68	13.31 ± 0.029
5	3.389681	-31	4.0 ± 0.22	13.06 ± 0.015
6	3.390156	2	1.6 ± 0.66	12.89 ± 0.076
7	3.390182	4	22.7 ± 0.64	14.09 ± 0.013
8	3.390781	44	19.7 ± 0.83	14.10 ± 0.019
9	3.391200	73	11.5 ± 0.68	13.54 ± 0.043
10	3.391548	97	12.8 ± 0.49	13.38 ± 0.021

**Fig. 2.** The best-fit Voigt profile of Ly α (cyan line) to the continuum-normalized ESPRESSO data (black line) for the absorption seen at $z_{\text{abs}} = 3.3901$. The best fitting H I column density is $\log N(\text{H I}) = 21.35 \pm 0.12$. The shaded cyan region denotes the range of profiles from the error on $\log N(\text{H I})$.

gle component profile, thus excluding the weak components 1, 2, and 5 from the ESPRESSO fit (Table 1; components 1 and 4 from UVES). However, we emphasize that these three weak components contribute minimally to the total column densities, and our derived total column densities are consistent with Molaro et al. (2000). Thus, while in Table 3 we conservatively assume $\log N(\text{Si II})$ is a lower limit as components 1 and 2 are severely blended, it is likely that they have little contribution to the total column density of Si II. Ignoring these missing components would imply a total $\log N(\text{Si II}) = 14.99 \pm 0.217$ from ESPRESSO.

Despite the $\approx 2\times$ lower S/N in the ESPRESSO data, the errors on the ESPRESSO total ion column densities are only $\approx 2\times$

higher than those of UVES. However, we emphasize that the number of components used in the fitting of the low ions and C IV profiles are not identical, preventing a fair comparison of the errors due to the degeneracy in component structure. Taking the redshifts of the fitted components for the ions Al II, Fe II, and C IV from ESPRESSO and fixing them in the UVES profile fitting results in both b_{turb} and $\log N$ being generally consistent when the same number of components are used in the fitting (Tables 4 and 5; for low ions and C IV respectively). We exclude Si II from the comparison due to the artefact seen in the UVES data. Figure 5 shows the distribution of errors on b_{turb} (top panel) and $\log N$ (bottom panel) for this alternative fit. While the errors on the UVES fits typically vary between $\approx 0.25 - 4.0\times$ that of ESPRESSO, the distribution of errors are comparable in size between the two datasets. Therefore, the combination of lower S/N but higher resolution does not significantly change the precision of fitting the same absorption line profile model. However, the combination of complex absorption profiles with either the lower S/N of the ESPRESSO data or lower resolution of UVES implies that the parameter space of the fitting process becomes highly degenerate and thus χ^2 minimization techniques may not converge on similar profiles fitted.

The two sets of data span two decades and we checked for a temporal evolution in the column density of the individual profiles' components by refitting the UVES Fe II and Al II lines with the same five components used to fit the ESPRESSO data. While keeping z and b_{turb} fixed, $\log N$ was refit for the UVES data (Tables 6). No significant evolution in column densities was detected. Within 1σ , all $\log N(\text{Fe II})$ for each fitted component in the UVES data were consistent with the equivalent component in ESPRESSO (Table 1), while only three components of the saturated Al II line were consistent within 1σ (the other two were within 2σ). We therefore cannot confirm potential changes in the column densities over the past two decades.

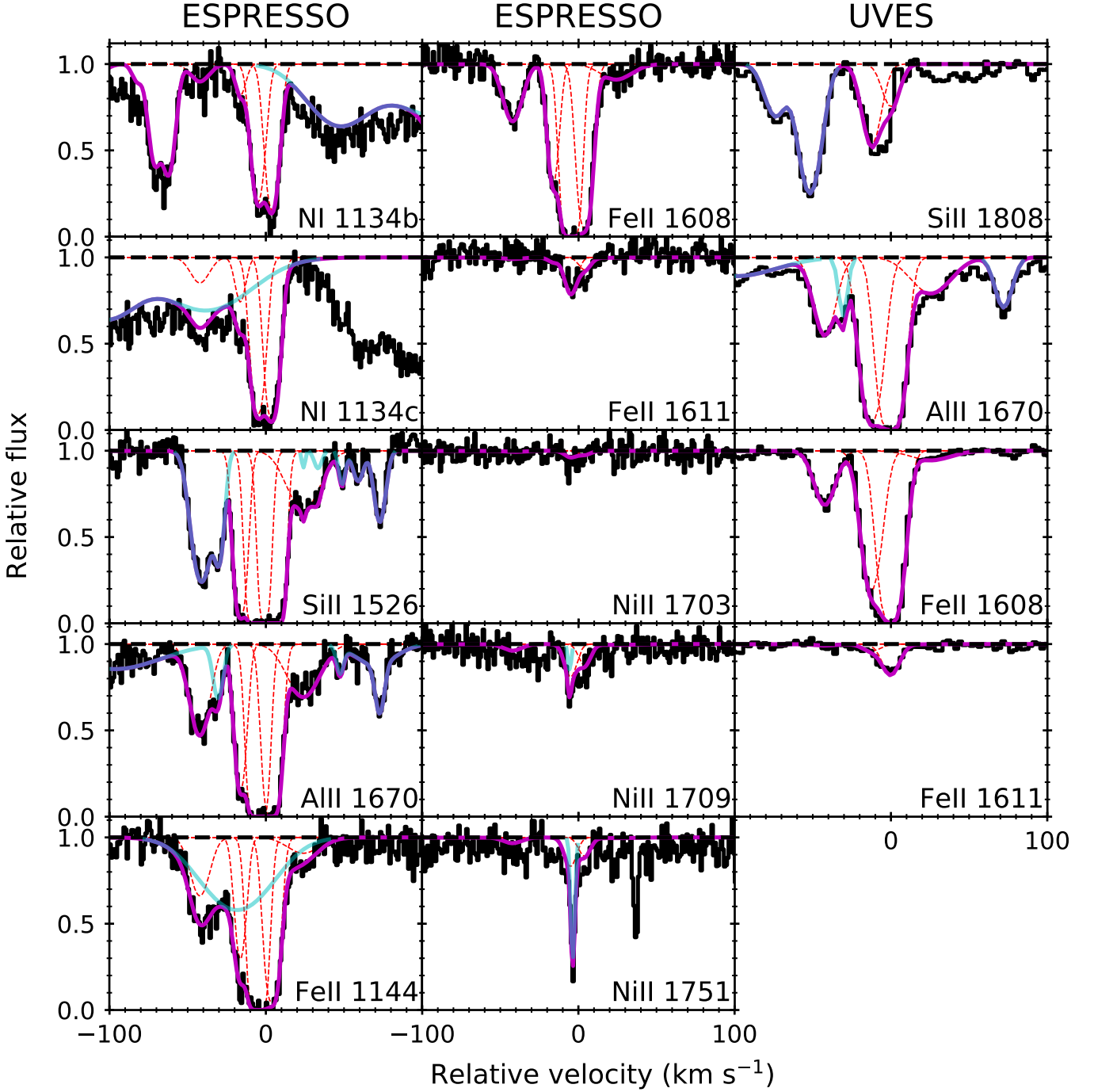


Fig. 3. Velocity profiles of key low-ionization absorption lines (labelled in the bottom right corner of each panel) detected within the continuum-normalized data (black lines) of QSO J0003–2603. The panels of the left two columns of the figure denote data from ESPRESSO, while the rightmost column shows the absorption lines of the UVES data. The solid magenta curve denotes the complete Voigt profile fitted to the data, while the red dashed lines denote the components that constitute the fit. Overplotted in cyan are the blended components. Although the profile for N I λ 1134.1 Å was not fit due to uncertain continuum blueward of the line, the expected profile shape based on the fits of the other two triplet lines (λ 1134.4 Å [1134b] and λ 1135.0 Å [1134c]) is shown in the N I 1134b panel at ≈ -70 km s $^{-1}$.

Table 3. Total column densities

Instrument	$\log N(\text{C IV})$	$\log N(\text{N I})$	$\log N(\text{Si II})$	$\log N(\text{Al II})$	$\log N(\text{Fe II})$	$\log N(\text{Ni II})$
ESPRESSO	14.70 ± 0.021	14.63 ± 0.015	> 15.01	13.44 ± 0.040	14.75 ± 0.018	13.42 ± 0.060
UVES	14.71 ± 0.007	...	> 15.12	13.47 ± 0.022	14.76 ± 0.015	...

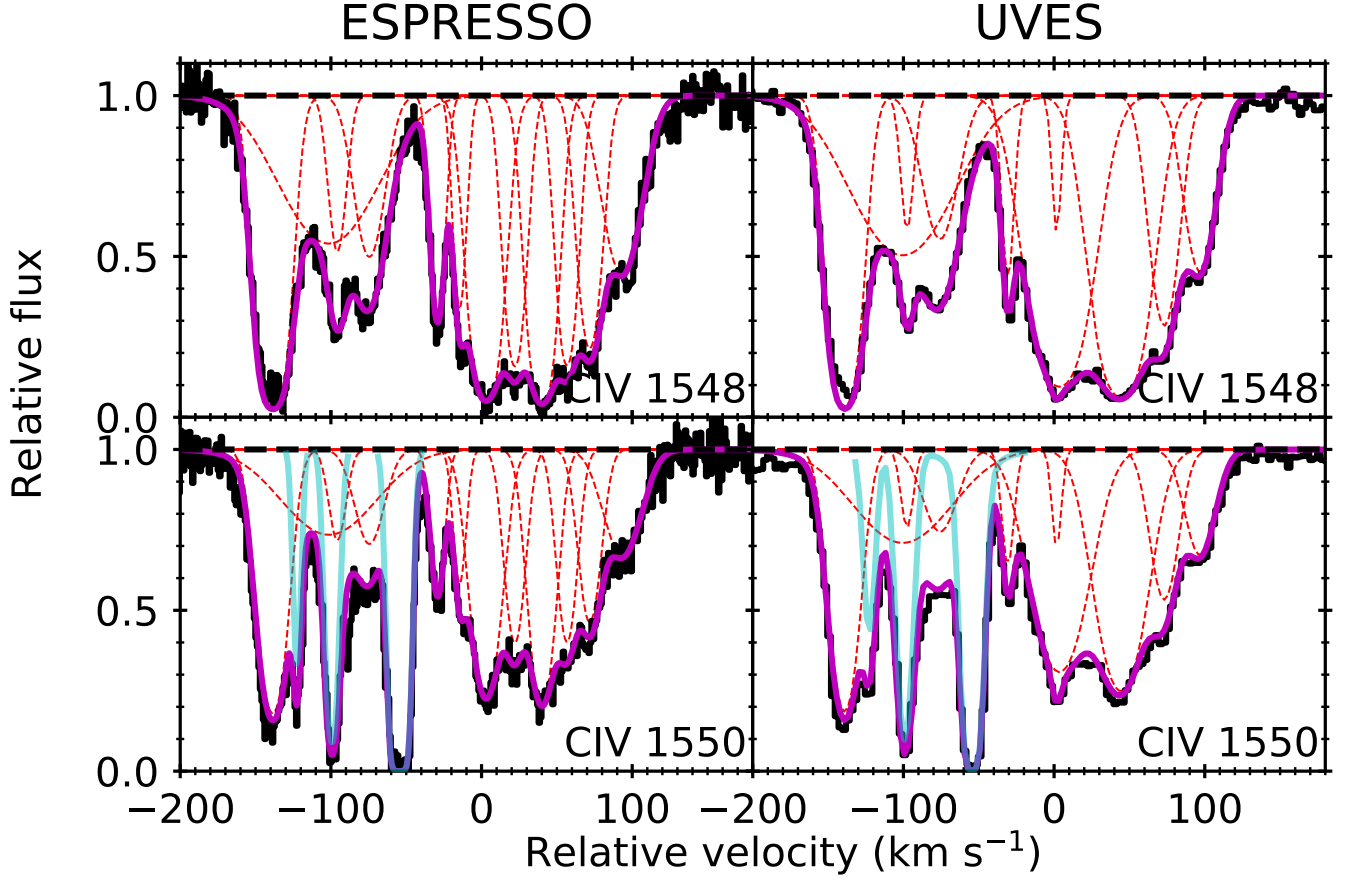


Fig. 4. Velocity profiles of the C iv doublet absorption seen in the ESPRESSO (left column) and UVES (right column) data of QSO J0003–2603. Notation is the same as in Figure 3.

Table 4. Fitted UVES Voigt profile parameters for low ions using the same five components’ redshifts of the ESPRESSO fit from Table 1

Comp.	z	Δv (km s ⁻¹)	b_{urb} (km s ⁻¹)	$\log N(\text{Al II})$	$\log N(\text{Fe II})$
1	3.389512	-42	8.5 ± 0.27	12.12 ± 0.017	13.39 ± 0.017
2	3.389892	-16	4.3 ± 0.12	12.49 ± 0.018	13.60 ± 0.019
3	3.390056	-5	6.0 ± 0.16	12.97 ± 0.035	14.42 ± 0.022
4	3.390188	4	4.6 ± 0.11	12.89 ± 0.036	14.19 ± 0.021
5	3.390481	24	15.2 ± 1.13	12.05 ± 0.033	12.81 ± 0.086

Table 5. Fitted UVES Voigt profile parameters for C iv using the same twelve components’ redshifts of the ESPRESSO fit from Table 2

Comp.	z	Δv (km s ⁻¹)	b_{urb} (km s ⁻¹)	$\log N(\text{C IV})$
1	3.388100	-139	11.2 ± 0.11	13.95 ± 0.004
2	3.388645	-101	43.8 ± 1.05	13.84 ± 0.014
3	3.388729	-96	4.3 ± 0.43	12.86 ± 0.028
4	3.389040	-74	14.1 ± 0.68	13.29 ± 0.029
5	3.389703	-29	5.7 ± 0.22	13.25 ± 0.012
6	3.389918	-15	5.4 ± 0.64	13.17 ± 0.083
7	3.390172	3	11.5 ± 1.28	13.90 ± 0.046
8	3.390453	22	8.2 ± 1.61	13.41 ± 0.184
9	3.390717	40	16.2 ± 1.84	14.06 ± 0.044
10	3.390960	57	4.7 ± 1.22	12.98 ± 0.186
11	3.391181	72	10.3 ± 0.69	13.59 ± 0.037
12	3.391497	93	13.8 ± 0.52	13.43 ± 0.020

4. Conclusions

This paper presents an analysis of the performance of ESPRESSO’s high spectral resolution, 4×2 binning mode (HR42) for observing faint quasars. Using four hours of on-target integration, we observed the quasar QSO J0003–2603 (AB magnitude $R = 18.5$ mag). An archival spectrum of the same quasar obtained with UVES for approximately the same exposure time allows one to compare ESPRESSO’s performance at extracting properties of an intervening DLA absorber. Despite having $\approx 2\times$ smaller S/N (per pixel) than the UVES spectra (Figure 1), the ESPRESSO HR42 mode observations were able to recover column densities and absorption profiles to nearly the same precision as the UVES data. For complex absorption profiles with many overlapping narrow features (such as the typical C iv profiles seen in strong Ly α absorbers), fitting Voigt profiles becomes degenerate with the modest S/N of our ESPRESSO data. The low ESPRESSO throughput below $\lambda \approx 5000$ Å prevents accurate continuum fitting and modelling of lines. The

Table 6. Fitted UVES component column densities using fixed ESPRESSO b_{turb} and z from Table 1

Ion	$\log N_{\text{Comp. 1}}$	$\log N_{\text{Comp. 2}}$	$\log N_{\text{Comp. 3}}$	$\log N_{\text{Comp. 4}}$	$\log N_{\text{Comp. 5}}$
Al II	12.15 ± 0.013	12.31 ± 0.018	13.18 ± 0.068	12.90 ± 0.026	12.06 ± 0.018
Fe II	13.37 ± 0.018	13.60 ± 0.015	14.59 ± 0.024	14.08 ± 0.017	12.99 ± 0.060

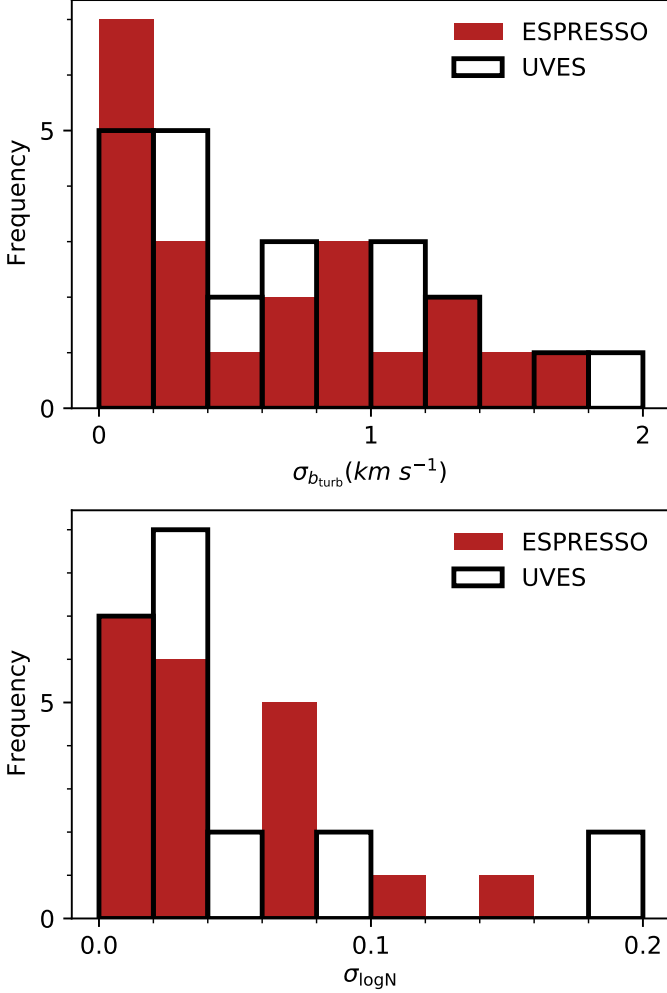


Fig. 5. Distributions of the errors on the fitted components' b_{turb} (top panel) and $\log N$ (bottom panel) for ions Al II, Fe II, and C IV from ESPRESSO (solid red bars) and UVES (hollow black bars) fits assuming the same number of components as the ESPRESSO fits for the respective ions (Tables 1 and 2). The UVES distributions show the errors derived from fitting the same redshift components as used in the ESPRESSO fits in order to provide an equal comparison. Despite the lower S/N in the ESPRESSO data, the errors on the component fits for ESPRESSO are similar in magnitude as those of UVES.

higher resolving power of ESPRESSO ($R \approx 136\,700$) allowed to identify additional narrow (i.e., small turbulent component of the Doppler broadening parameter) substructure within the metal absorption profiles that were missed by the typical UVES setup used for observing DLAs ($R \approx 48\,000$) despite the $\approx 2\times$ lower S/N (per pixel). Whilst UVES can achieve a resolving power beyond 100 000, in order to match the same S/N depth as ESPRESSO (after accounting for differing pixel size), observations with UVES would require double the exposure time. Furthermore, the spectral resolution element of

UVES would not be properly sampled at this resolution. Thus ESPRESSO's HR42 mode provides an optimal combination of extended wavelength coverage, resolving power, and observing efficiency above 5000 Å that UVES cannot obtain.

In summary, ESPRESSO's HR42 mode can provide additional stability and $\approx 3\times$ the spectral resolving power with a comparable performance to UVES beyond $\lambda \geq 5000$ Å for analysing quasar absorption line systems. As the equivalent width of a line scales as FWHM divided by S/N, the HR42 mode of ESPRESSO would be an ideal avenue for searching for weaker lines, such as C I, Si I, and rare elements, typically not easily identified with UVES. The increased resolution and sensitivity of the HR42 mode combined with the stability and precise wavelength calibration of ESPRESSO enables precision physics and cosmological experiments (Iršič et al. 2017; Cooke et al. 2020; Schmidt et al. 2021), and observations quantifying isotopic ratios and gas temperatures of individual absorbers (Narayanan et al. 2006; Cooke et al. 2015; Welsh et al. 2020; Noterdaeme et al. 2021) whilst minimizing observing time requirements using a single UT.

Acknowledgements. We are grateful for assistance, discussions and comments provided by Ryan Cooke, Valentina D'Odorico, Alain Smette, and Louise Welsh that significantly improved this manuscript, and for the comments from the anonymous referee that helped improve the clarity of the text. We are thankful for the ESPRESSO observations that were supported by and collected at the European Southern Observatory under ESO programme 60.A-9801(W).

References

- Berg, T. A. M., Ellison, S. L., Prochaska, J. X., Venn, K. A., & Dessauges-Zavadsky, M. 2015, *MNRAS*, 452, 4326
- Berg, T. A. M., Ellison, S. L., Venn, K. A., & Prochaska, J. X. 2013, *MNRAS*, 434, 2892
- Cooke, R., Welsh, L., Fumagalli, M., & Pettini, M. 2020, *MNRAS*, 494, 4884
- Cooke, R. J., Pettini, M., & Jorgenson, R. A. 2015, *ApJ*, 800, 12
- Cooke, R. J., Pettini, M., & Steidel, C. C. 2018, *ApJ*, 855, 102
- Cupani, G., D'Odorico, V., Cristiani, S., et al. 2019, in *Astronomical Society of the Pacific Conference Series*, Vol. 521, *Astronomical Data Analysis Software and Systems XXVI*, ed. M. Molinaro, K. Shorridge, & F. Pasian, 362
- De Cia, A. 2018, *A&A*, 613, L2
- Dekker, H., D'Odorico, S., Kaufer, A., Delabre, B., & Kotzlowski, H. 2000, in *Society of Photo-Optical Instrumentation Engineers (SPIE) Conference Series*, Vol. 4008, *Optical and IR Telescope Instrumentation and Detectors*, ed. M. Iye & A. F. Moorwood, 534–545
- Ellison, S. L., Ryan, S. G., & Prochaska, J. X. 2002, in *Astrophysics and Space Science Library*, Vol. 274, *New Quests in Stellar Astrophysics: the Link Between Stars and Cosmology*, ed. M. Chávez, A. Bressan, A. Buzzoni, & D. Mayya, 207–210
- Freudling, W., Romaniello, M., Bramich, D. M., et al. 2013, *A&A*, 559, A96
- Iršič, V., Viel, M., Haehnelt, M. G., et al. 2017, *Phys. Rev. D*, 96, 023522
- Krogager, J. K., Noterdaeme, P., O'Meara, J. M., et al. 2018, *A&A*, 619, A142
- Levshakov, S. A., Molaro, P., Centurión, M., et al. 2000, *A&A*, 361, 803
- Lu, L., Sargent, W. L. W., Barlow, T. A., Churchill, C. W., & Vogt, S. S. 1996, *ApJS*, 107, 475
- Molaro, P., Bonifacio, P., Centurión, M., et al. 2000, *ApJ*, 541, 54
- Murphy, M. T. & Cooksey, K. L. 2017, *MNRAS*, 471, 4930
- Murphy, M. T., Kacprzak, G. G., Savorgnan, G. A. D., & Carswell, R. F. 2019, *MNRAS*, 482, 3458
- Narayanan, A., Misawa, T., Charlton, J. C., & Ganguly, R. 2006, *AJ*, 132, 2099
- Neeleman, M., Prochaska, J. X., & Wolfe, A. M. 2015, *ApJ*, 800, 7
- Noterdaeme, P., Balashev, S., Ledoux, C., et al. 2021, *A&A*, 651, A78
- Pepe, F., Cristiani, S., Rebolo, R., et al. 2021, *A&A*, 645, A96

- Pepe, F. A., Cristiani, S., Rebolo Lopez, R., et al. 2010, in Society of Photo-Optical Instrumentation Engineers (SPIE) Conference Series, Vol. 7735, Ground-based and Airborne Instrumentation for Astronomy III, ed. I. S. McLean, S. K. Ramsay, & H. Takami, 77350F
- Schmidt, T. M., Molaro, P., Murphy, M. T., et al. 2021, A&A, 646, A144
- Smette, A., Sana, H., Noll, S., et al. 2015, A&A, 576, A77
- Tchernyshyov, K., Meixner, M., Seale, J., et al. 2015, ApJ, 811, 78
- Welsh, L., Cooke, R., Fumagalli, M., & Pettini, M. 2020, MNRAS, 494, 1411
- Wolfe, A. M., Gawiser, E., & Prochaska, J. X. 2005, ARA&A, 43, 861